Ceramics International 47 (2021) 33525–33536

Contents lists available at ScienceDirect

Ceramics International

journal homepage: www.elsevier.com/locate/ceramint

Non-linear mechanical properties and dynamic response of silicon nitride bioceramic

Xiaoyu Du [a,*], Gurdial Blugan [b], Tina Künniger [c], Seunghun S. Lee [a], Liliya Vladislavova [b], Stephen J. Ferguson [a]

[a] Institute for Biomechanics, ETH Zurich, Zurich, Switzerland
[b] Laboratory for High Performance Ceramics, Empa, Swiss Federal Laboratories for Materials Science and Technology, Dubendorf, Switzerland
[c] Laboratory for Cellulose & Wood Materials, Empa, Swiss Federal Laboratories for Materials Science and Technology, Dubendorf, Switzerland

ARTICLE INFO

Keywords:
Porous silicon nitride
Damping
Impact
Spinal implant
Mechanical properties

ABSTRACT

Natural spinal tissues have unique dynamic properties and it is crucial to investigate the full dynamic response of spinal implants and related biomedical materials to ensure compatibility with the host tissue. Silicon nitride is a promising bioceramic for spinal implants. In this study, the mechanical properties and dynamic response of silicon nitride were comprehensively evaluated using novel and efficient testing methods, at both the material and structural level. The correlation between mechanical properties and porosity was investigated and the results showed that Young's modulus and compressive strength decreased non-linearly as porosity increased. Both the compressive strength (100.35 ± 3.39 MPa) and fracture toughness (1.06 ± 0.06 MPa·m$^{1/2}$) of the porous silicon nitride samples (~70% porosity) can be considered sufficient for load bearing purposes as a substitute for trabecular bone. Moreover, the results from a drop tower test showed that the average ultimate strength of the scaffolds under an impact loading was significantly lower than the strength under quasi-static compression. Nevertheless, this value is still comparable to that of trabecular bone. Regarding damping capacity, the results of free damped vibration tests of cantilever beams showed that a silicon nitride beam has a higher damping ratio ($0.17\% \pm 0.01\%$) than a zirconia beam ($0.13\% \pm 0.01\%$), which indicates that ceramics with similar Young's moduli can have different energy dissipating capacities. However, both dense and porous silicon nitride showed a low energy dissipation, substantially lower than natural spinal tissues. Overall, dense silicon nitride possesses a high stiffness, and altering the porosity of silicon nitride is one option to tailor its mechanical properties towards those of trabecular bone, however, more effort is required to increase its damping capacity, if this is a desired trait.

1. Introduction

Silicon nitride possesses a variety of excellent properties, such as strength, fracture toughness, and osteoconductivity, as well as an anti-bacterial effect. These are essential for spinal implant development [1–3]. Silicon nitride was first used in anterior intervertebral spacers in a small clinical trial in Australia in 1986, and the follow-up results at the approximate time points of 1, 5, 10, and 30 years were presented [4,5]. The 30-year follow up of 5 patients, using CT and standing radiography, showed that bone fusion and osseointegration with the surrounding tissue was achieved in 100% of the patients. Overall, this long-term clinical study demonstrated the biocompatibility, osseointegration, and osteogenic capability of silicon nitride. Moreover, Kersten et al. [2] compared the bone formation capacity between silicon nitride and polyether ether ketone (PEEK) for lumbar interbody fusion surgeries using a caprine model. The results demonstrated that silicon nitride spacers were not inferior to PEEK, with respect to bone-implant contact and biodynamic stability, and better in promoting arthrodesis than PEEK. Silicon nitride was cleared to be used as interbody cages by both CE and FDA in 2008, based on animal studies and standard compliance requirements [6]. In addition, extensive clinical results have demonstrated the effectiveness of silicon nitride as spinal implants in the treatment of symptomatic degenerative cervical and lumbar disc disorders [1,7,8].

However, the high Young's modulus of silicon nitride may cause stress shielding and lead to bone atrophy. As a solution, macroporous

* Corresponding author.
E-mail address: xiaodu@ethz.ch (X. Du).

https://doi.org/10.1016/j.ceramint.2021.08.261
Received 4 August 2021; Received in revised form 13 August 2021; Accepted 21 August 2021
Available online 24 August 2021

ceramics with a wide range of porosity have been extensively applied in bone implants to reduce stress shielding and promote osseointegration [9,10]. The design of a porous structure provides a possible avenue to reduce the stiffness of implants, but usually at the expense of decreased strength. However, sufficient strength is also required to ensure the stability and safety of the implant [11,12]. Therefore, to add valuable data for designing optimal spinal implants, it is essential to investigate the correlation between mechanical properties and porosity in silicon nitride bioceramics.

It is well-known that natural spinal tissues have unique dynamic properties. Vertebral bone and intervertebral discs show a frequency-dependent response, producing non-linear deformations under different loading conditions. For instance, intervertebral discs act as cushions between the adjacent vertebrae, producing corresponding deformations under various loads to absorb shock energy and to stabilize the spine [13]. Conversely, discs can be damaged and/or amplify energy transfer to surrounding fragile bone by enhanced mechanical stimulation (i.e. resonance) at certain vibration frequencies [14]. Biomechanical evidence also points to a critical role of damping in the function of implants for reconstruction of the spinal column [14–16]. Thus, investigating the full dynamic response of spinal implants and related biomedical materials is crucial to ensure compatibility with the host tissue.

Present implant evaluation methods are typically aimed at evaluating only the quasi-static mechanical properties of the device [17]. Still, there is no efficient test method and standard to evaluate the dynamic response of biomaterials for spinal implants, and the application of such methods to characterize and to compare biomaterials. Therefore, in this study, the mechanical properties and dynamic response of silicon nitride have been evaluated using novel and efficient testing methods, at both the material and structural level. Moreover, the relationship between the mechanical properties and porosity of silicon nitride scaffolds was determined.

2. Materials and methods

2.1. Material preparation

Silicon nitride beam samples (denoted as SN) doped with alumina and yttria additives were sintered followed by diamond grinding to give a final dimension of 45 mm × 4 mm × 0.5 mm for the free decay vibration test. Monolithic 3 mol% yttria-doped tetragonal zirconia polycrystal (3Y-TZP) beams (denoted as TZP) were also fabricated as a control group. Porous silicon nitride ceramics exhibiting a uniform and partly accessible porous structure were fabricated by SINTX Technologies Inc. (Salt Lake City, Utah, USA).

2.2. Characterization of silicon nitride scaffolds

The morphology and microstructure of the scaffolds were observed by scanning electron microscopy (SEM, FEI Quanta 200F). Prior to examination, each sample was coated with Pt/Pd (80/20) using a sputter coater (CCU-010, Safematic). An energy dispersive X-ray analyzer (EDX, Rontec, Germany) was used to semi-quantitatively investigate the chemical composition of the silicon nitride beam and zirconia beam samples.

The porosity of porous silicon nitride ceramics was determined from the following equation:

$$P = 1 - \frac{\rho}{\rho_0} \tag{1}$$

where ρ is the apparent density of porous ceramics and ρ_0 is the bulk density of the equivalent solid matrix material (without pores), which is 3.26 $g{\cdot}cm^{-3}$ for the silicon nitride in our study. Porous specimens were scanned using a micro-CT 100 (7.4 μm voxel size, 70 kVp, 114 μm, 8 W, Scanco Medical, Brüttisellen, Switzerland) to observe the structure, in terms of pore shapes and distribution. Morphometric parameters, such as bone volume fraction (BV/TV), were calculated using ImageJ software to validate the porosity calculated from equation (1).

2.3. Free decay vibration test of thin silicon nitride beam

The fundamental vibration frequency of the silicon nitride beam was measured experimentally by using a non-contact vibration measurement technique. The damping ratio was calculated from the envelope of the free vibration response. Specifically, the beam sample was clamped vertically at one end (5 mm), while the other end was free. The initial condition was to put a weight at the free end and release the weight. When the beam vibrated, a high-speed camera (MotionPro Y8–S3, Integrated Design Tools, Ltd, UK) was used to capture the movement of the free end at 5000 frames/seconds. Then, an open-source software Tracker (open source physics, comPADRE.org) was used to extract the displacement of the free end in the vertical direction. The vibrations at the free end mainly depend on the stiffness and damping of the cantilever beam. The vibration displacement (y data) shows the response of an underdamped second-order system. A curve fitting function in MATLAB (R2018a, MathWorks, Massachusetts, USA) was then used to fit a custom equation ($y = Ae^{-\alpha t}\cos(w_d t + \phi)$), including the exponential decay of the peaks of the y data and the periodical displacement. The coefficient of the exponential term represents the rate of decay of the free vibration response and is directly related to the damping ratio of the cantilever beam [18]. The captured data was used to determine the damped frequency and the damping ratio of the cantilever using the following equation (2).

$$Damping\ ratio:\ \xi = \frac{\alpha}{\sqrt{w_d^2 + \alpha^2}} \tag{2}$$

where α is the decay factor and w_d is the damped frequency.

2.4. Dynamic mechanical tests of dense and porous silicon nitride beam

The dynamic Young's modulus (E) for dense and porous silicon nitride beams with a rectangular section (3 × 4 mm) was measured by sonic excitation using a Grindo-Sonic Mark 5 (Lemmens, Germany) on 45 mm × 3 mm × 4 mm specimens. The dense beam had nearly 0% porosity, whilst the porous beam had approx. 70% porosity. Furthermore, the damping capacity and dynamic Young's modulus of the porous silicon nitride beam were also assessed using a dynamic mechanical analyzer (DMA, TA Instruments, New Castle, USA) in a clamped 3-point bending mode, with a span length of 38 mm. The temperature was set to 37 °C. All tests were conducted as frequency sweeps from 0.1 Hz to 100 Hz and 0.005% strain as a level within the linear response. The complex modulus E*, which encompasses the elastic (storage modulus E′) and viscous (loss modulus E″) response and the damping coefficient or loss factor (Tan delta) were measured. E* is a measure of resistance to deformation, while Tan delta expresses the energy dissipated as heat during deformation [19].

2.5. Fracture toughness tests of dense and porous silicon nitride beam

Fracture toughness of dense and porous silicon nitride beams was measured on 45 mm × 3 mm × 4 mm specimens using the single-edge V-notch beam (SEVNB) method. The notches were inserted using a specifically constructed notching machine and the final notching was performed using 1 μm diamond paste and a steel razor blade [20]. Then the samples with V-notch were compressed in a 4-point bending mode on a materials testing machine (Zwick/Roell, 5 kN). The crosshead displacement speed for the dense silicon nitride bar was 1 mm/min, while the speed for porous silicon nitride with ~70% porosity was 0.7 mm/min. The fracture toughness was calculated from the following

equation:

$$K_{IC} = \frac{F_c}{B\sqrt{W}} \cdot \frac{S_1 - S_2}{W} \cdot \frac{3\sqrt{\alpha}}{2(1-\alpha)^{1.5}} Y^* \quad (3)$$

with: $Y^* = 1.9887 - 1.326\alpha - (3.49 - 0.68\alpha + 1.35\alpha^2)\alpha(1-\alpha)(1+\alpha)^{-2}$

where F_c is the fracture load, S_1 is outer span, S_2 is inner span, B is specimen width, W is specimen height, a is notch depth, α is a/W, and Y is stress intensity shape factor.

2.6. Quasi-static compression test of cylindrical silicon nitride scaffolds with different porosity

Porous cylindrical silicon nitride scaffolds (height 16 mm, diameter 8 mm) were fabricated. The Young's modulus, compressive strength, and ultimate strain of the scaffolds from different porosity groups were tested using a materials testing machine (Instron E10000, 10 kN load cell, Instron, High Wycombe, UK) at a compression speed of 0.01 mm/s.

A mathematical model developed by Nielsen [21] was used to describe the porosity dependence of Young's modulus for porous silicon nitride scaffolds. In a porous ceramic, the pores can be considered as a phase whose mechanical properties are equal to zero. Thus, the effective Young's modulus is given by the following equation:

$$E = \frac{(1-P)^2}{1 + \left(\frac{1}{S} - 1\right) \cdot P} \cdot E_s \quad (4)$$

where P is the porosity of the materials, and E and E_s denotes Young's modulus of the porous material and solid phases, respectively. The shape factor (S) is dependent on the pore geometry and distribution and it was determined by fitting the model to the measured values.

2.7. Dynamic loading test of porous silicon nitride scaffolds

Two different cyclic loading protocols were applied at a constant displacement rate: cyclic loading to a predefined maximum displacement at each loading cycle, and progressive loading to a maximum displacement in increasing steps, with full unloading in between loading steps. Porous silicon nitride cylinder samples of 76% porosity with a dimension of 4 mm radius and 16 mm height were used and the experiments were performed on a dynamic materials testing machine (Instron E10000, 10 kN load cell, Instron, High Wycombe, UK) in air and at room temperature.

2.8. Drop tower test to evaluate the mechanical behavior of porous silicon nitride scaffolds under impact loading

Samples of the 76% porosity group were impacted within a miniature drop tower [22]. The kinetic energy and impact velocities were prescribed by adjusting the impact mass and initial height. Based on preliminary experiments, an impact velocity of 1.7 m/s and impact energy of 250 mJ was chosen, since 250 mJ was found as an acceptable minimum energy required to induce total fracture in specimens. The impact force was measured using a piezoelectric load cell (Kistler 9321B, 50 kHz, Sindelfingen, Germany) which was fixed to the rigid steel base plate of the apparatus. A 2nd-order low pass Butterworth filter was used to filter out the high-frequency noise. The impact process was recorded by a high-speed video camera (MotionPro Y8–S3, Integrated Design Tools, Ltd, UK) at 50000 frames per second and a resolution of 512 × 48 pixels. Displacement of the superior illuminated aluminum endcap was tracked frame-by-frame using the open-source software Tracker (open source physics, comPADRE). The ultimate strength was analyzed using displacement and force data.

2.9. Statistical analysis

Each group had at least three samples and three separate experiments carried out to collect the data. The data were expressed as mean values ± standard deviations and analyzed by analysis of variance (ANOVA) using GraphPad Prism 8.2.0 software (GraphPad Software Inc, California, USA). The level of statistical significance was set at $p \leq 0.05$. All the error bars in the figures correspond to the SE of the mean to indicate the uncertainty for each measurement.

3. Results

3.1. Free decay vibration test results of thin silicon nitride beam

Fig. 1 shows the surface morphologies of silicon nitride and zirconia samples, respectively. Since the beam sample was diamond ground, there were parallel machining marks on the surface of each sample. The EDX results confirmed the material composition of the silicon nitride and zirconia beams. Then, the damping ratio was calculated by means of the free vibration decay response of the cantilever beam. Fig. 2(A) shows the comparison of the free vibration response of the different cantilever beams. The free vibration amplitudes decayed faster for the SN beam than for the TZP beam. The exponent of the envelope curve was also higher for the SN beam, reflecting an increased damping ratio, which was in good agreement with the damping ratio calculated using the logarithmic decrement as given in Fig. 2 (C). The damping ratio of silicon nitride beam was 0.17% ± 0.01%, while the zirconia beam had a lower damping ratio of 0.13% ± 0.01%. For the damped frequency, the SN beam was also significantly higher than the TZP beam, as shown in Fig. 2 (B).

3.2. Mechanical properties comparison between dense and porous silicon nitride beam

The dynamic Young's modulus of the dense silicon nitride measured ultrasonically was 298.45 ± 1.08 GPa, which was around 11 times higher than that of the porous silicon nitride beam with 70% porosity (26.26 ± 1.23 GPa), as shown in Fig. 3 (C). Dynamic mechanical analysis testing results (Fig. 6) for the porous silicon nitride also showed that the complex modulus was in the range of 20 GPa–30 GPa and did not show a clear frequency dependence in the investigated frequency range. The loss factor was very small, indicating low energy dissipation. It should be noted that DMA machines are usually used to evaluate the viscoelastic behavior of polymers. Although there are some studies using DMA to test the damping properties of metals and ceramics [23–25], the data reliability should be carefully considered. Nevertheless, the results in this study still indicate low damping properties of the porous silicon nitride beam with 70% porosity.

The fracture toughness measured by SEVNB tests of dense silicon nitride and porous silicon nitride were 5.43 ± 0.09 MPa·m$^{1/2}$ and 1.06 ± 0.06 MPa·m$^{1/2}$, respectively. Notably, as show in Fig. 3 (A), the fracture toughness of porous silicon nitride was still higher than that of human trabecular bone. Fig. 4 (A) shows the V-notch of dense silicon nitride before testing, and the diameter of the notch was around 3 μm which functioned well as a pre-crack. The diameter of the notch for the porous silicon nitride was around 63 μm due to the porous structure. Fig. 4 (B, C, D) and (F, G, H) present images of dense and porous silicon nitride after SEVNB tests, respectively. We observed a relatively even fracture surface for the dense samples, while the fracture surface for the porous silicon nitride sample was uneven. The fracture mechanism for both was brittle fracture. In addition, although the porosity was up to 70%, the fractures toughness of the porous silicon nitride samples decreased around a factor of 5 compared to the dense samples. Fig. 5 shows cross-section SEM images of both dense and porous samples after SEVNB tests. We observed that porous silicon nitride samples have more

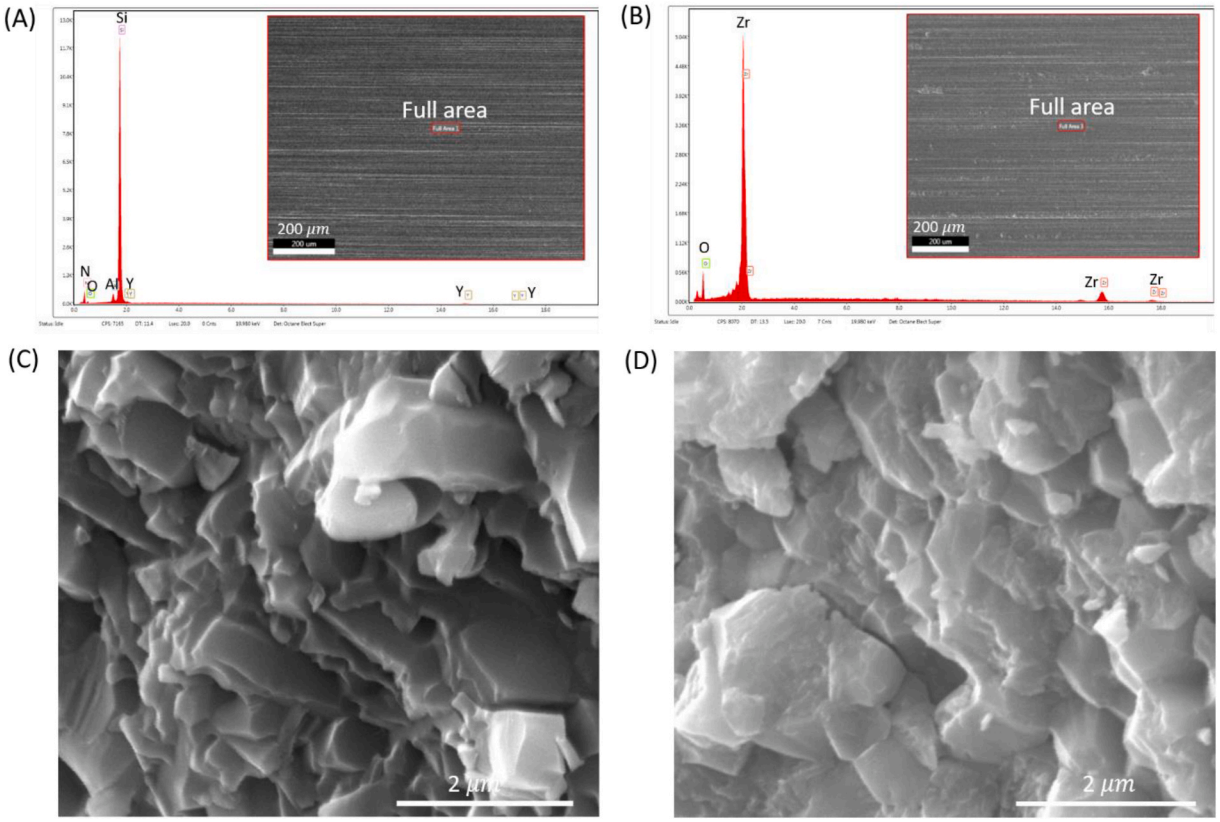

Fig. 1. SEM and EDX results of beam samples for (A) silicon nitride beam and (B) zirconia beam (The attached images show the region of EDX spot that was analyzed.); cross section SEM image of (C) silicon nitride beam and (D) zirconia beam. (For interpretation of the references to colour in this figure legend, the reader is referred to the Web version of this article.)

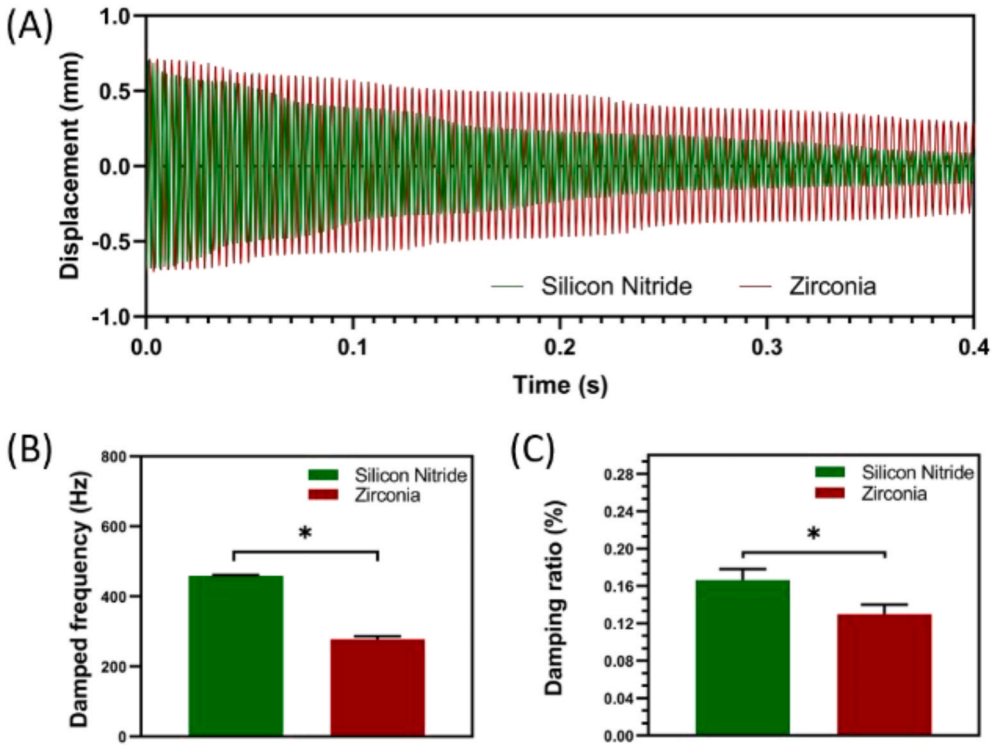

Fig. 2. (A) Representative graph of displacement vs. time curve, (B) Damped frequency, and (C) Damping ratio of the damped silicon nitride beam and zirconia beam (40 mm × 4 mm × 0.5 mm). (For interpretation of the references to colour in this figure legend, the reader is referred to the Web version of this article.)

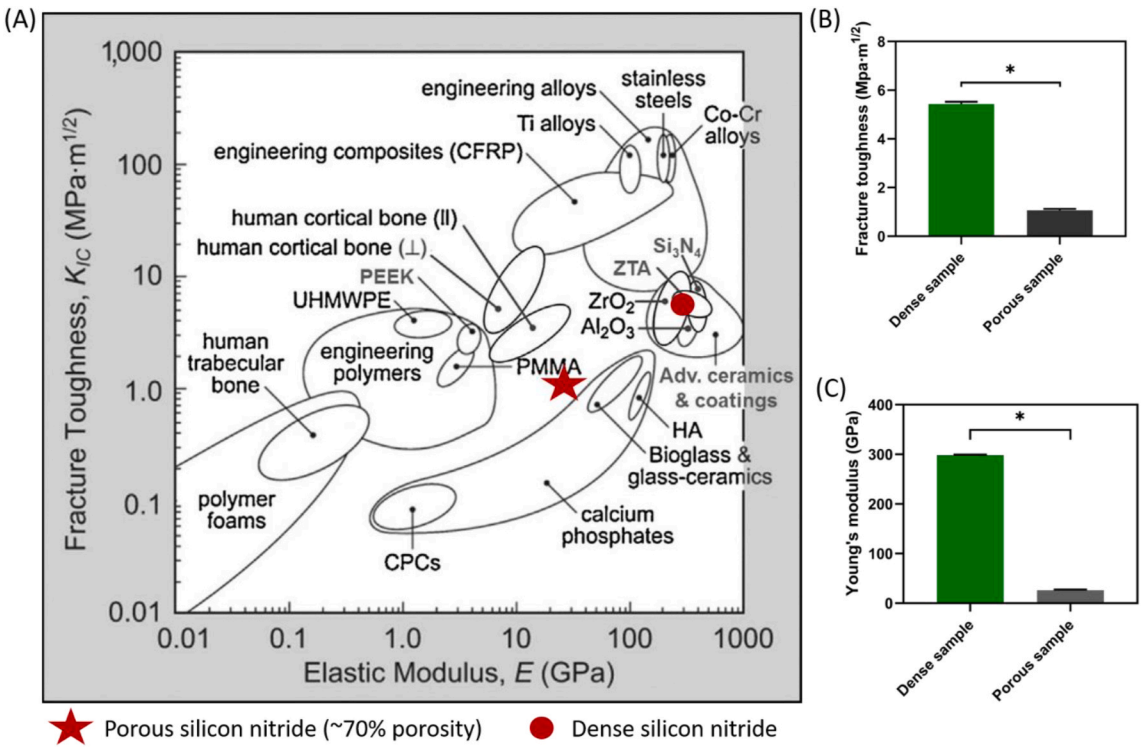

Fig. 3. (A) An Ashby diagram showing the elastic modulus and fracture toughness of bone tissue compared to biomaterials commonly used as orthopaedic implants. The mechanical properties of cortical bone are shown for loading parallel (//) and perpendicular (⊥) to the longitudinal anatomic axis. Adapted from Refs. [28,56] with permission from Springer Nature (copyright 2008) and Elsevier (copyright 2015). (B) Fracture toughness of dense silicon nitride and porous silicon nitride (~70% porosity) samples tested by the single-edge V-notch beam method. (C) Young's modulus of dense silicon nitride and porous silicon nitride (~70% porosity) samples tested by the sonic excitation method. (For interpretation of the references to colour in this figure legend, the reader is referred to the Web version of this article.)

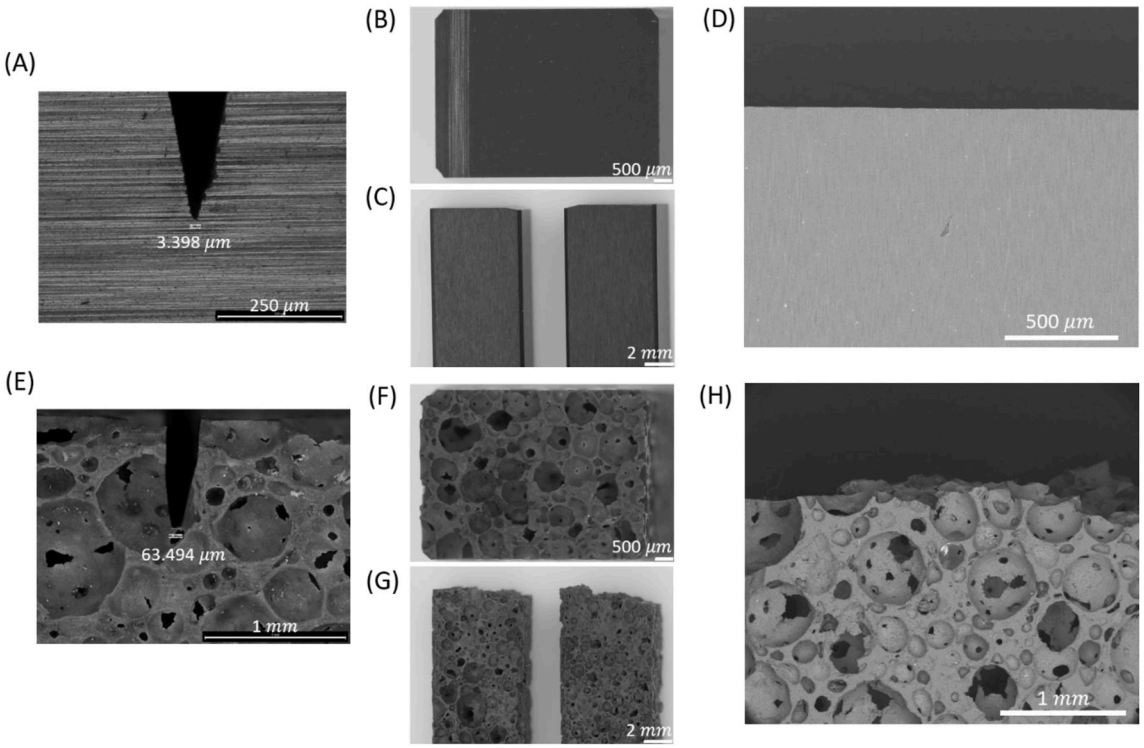

Fig. 4. Single-edge V-notch beam test: V-notch in (A) dense silicon nitride and (E) porous silicon nitride before bending test; Optical image of cross section after bending testing for (B) dense silicon nitride and (F) porous silicon nitride; Optical and SEM image after samples break for (C, D) dense silicon nitride and (G, H) porous silicon nitride.

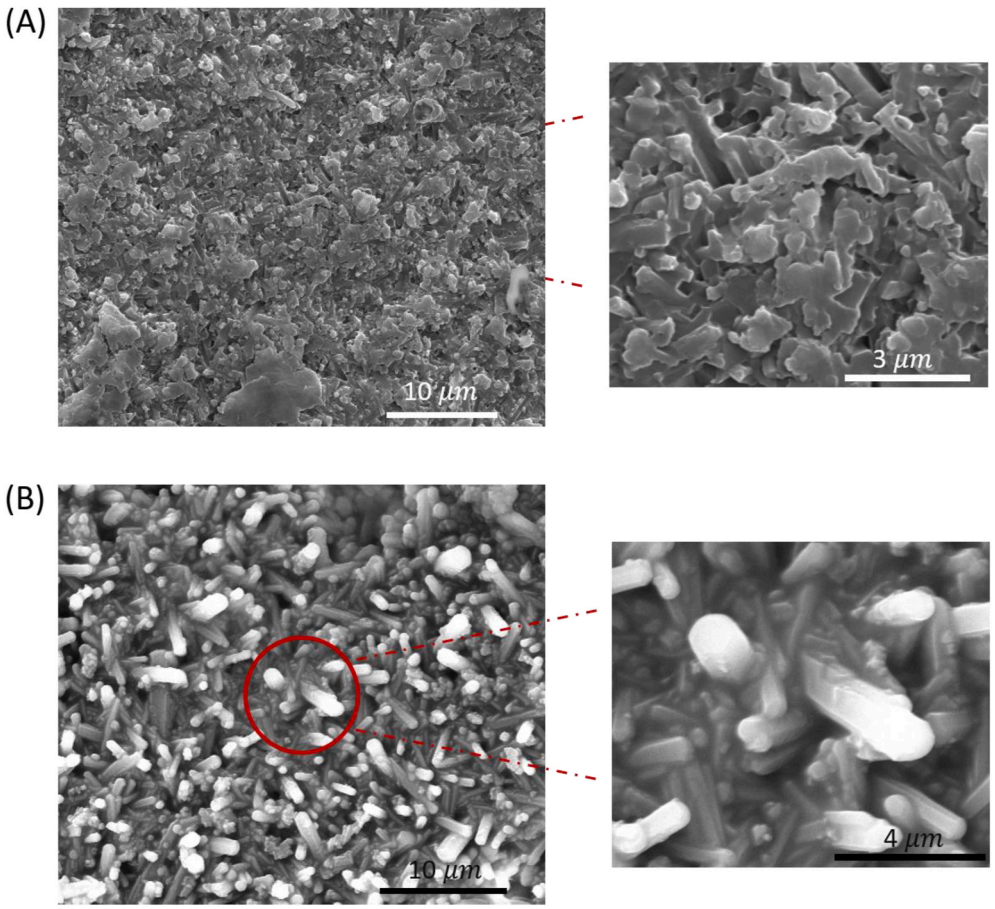

Fig. 5. SEM image of the cross section of (A) dense silicon nitride and (B) porous silicon nitride after single-edge V-notch beam tests. (For interpretation of the references to colour in this figure legend, the reader is referred to the Web version of this article.)

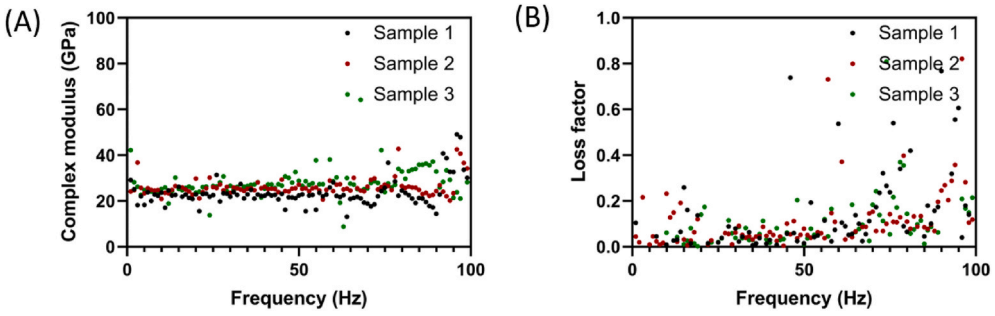

Fig. 6. DMA results of porous silicon nitride beam with ~70% porosity. (For interpretation of the references to colour in this figure legend, the reader is referred to the Web version of this article.)

elongated grains compared to dense silicon nitride.

3.3. Porosity dependence of Young' modulus and compressive strength

Fig. 7 shows optical and Micro-CT images of porous silicon nitride cylindrical samples. As can clearly be observed, the cavity area increased with the increasing porosity. Moreover, it possessed partly continuous and channel-like pore cavity structures. The compression results for silicon nitride with different porosity showed that Young's modulus, compressive strength, and ultimate strain decreased non-linearly as porosity increased, as shown in Fig. 8.

As for the elasticity model of porous materials, the shape factor (S) is dependent on the pore geometry and distribution, and its value is in the range from 0 to 1. Usually, shell-like pore networks and compact solid particles decrease the magnitude of S, whilst high shell-like solid networks and pore "pockets" of compact shapes increase the magnitude of S [26]. The experimental data obtained from our study was used to fit this mathematical model. The constant S = 0.4526 was determined, which is consistent with the semi-empirical laws.

We observed the fracture cross sections of the samples after compression failure. The silicon nitride samples are nearly 100% β-silicon nitride with an elongated grain structure, as shown in Fig. 9. The grains are randomly oriented, resulting in an isotropic microstructure. The brittle fracture morphologies indicated both inter-and *trans*-granular crack propagation.

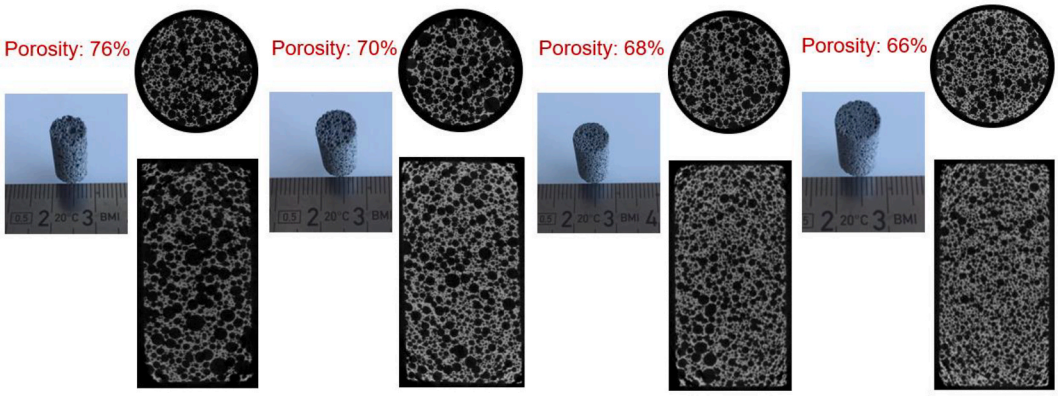

Fig. 7. Optical and Micro-CT image of porous silicon nitride cylinder, diameter:8 mm, height:16 mm. (For interpretation of the references to colour in this figure legend, the reader is referred to the Web version of this article.)

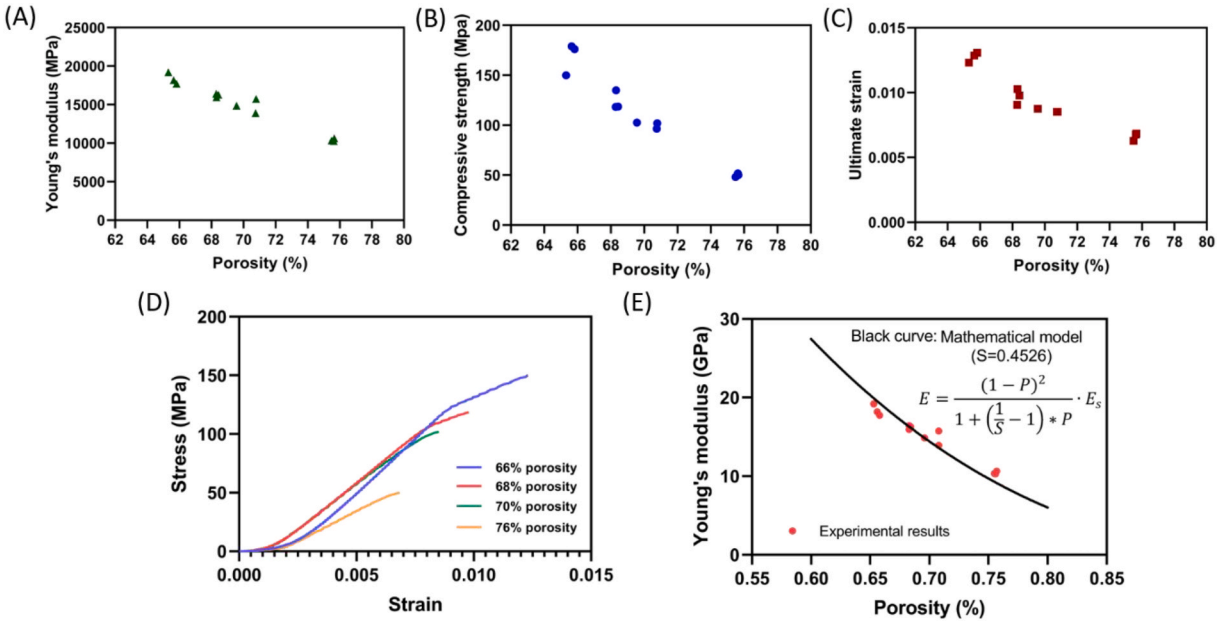

Fig. 8. Compression testing results of porous silicon nitride: (A) Young's modulus; (B) Compressive strength; (C) Ultimate strain; (D) Stress-strain curve, and (E) Comparison with the mathematical model. (For interpretation of the references to colour in this figure legend, the reader is referred to the Web version of this article.)

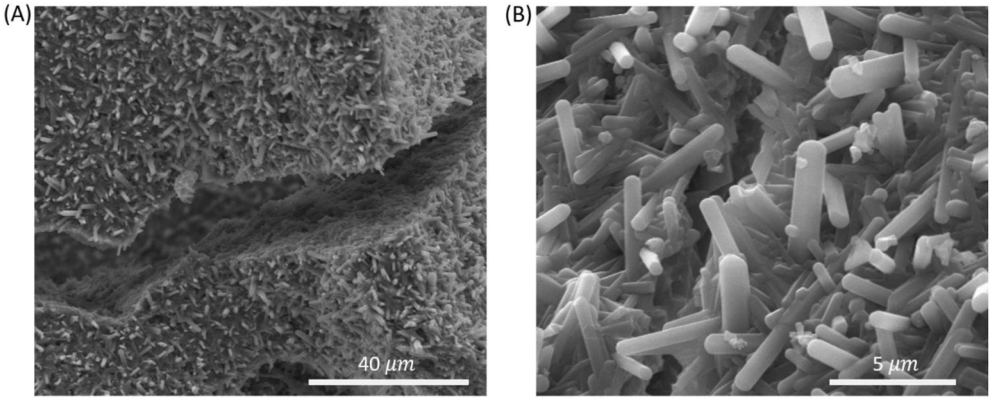

Fig. 9. Grain fracture morphology of porous silicon nitride after compression to failure.

3.4. Dynamic loading testing results of porous silicon nitride scaffolds

Fig. 10 (A, C) shows the stress vs. strain curve of porous silicon nitride scaffold under progressive loading. There is an elastic region within the strain range from 0 to 0.2%, where there was no energy dissipation and no permanent deformation. If the strain exceeded 0.2%,

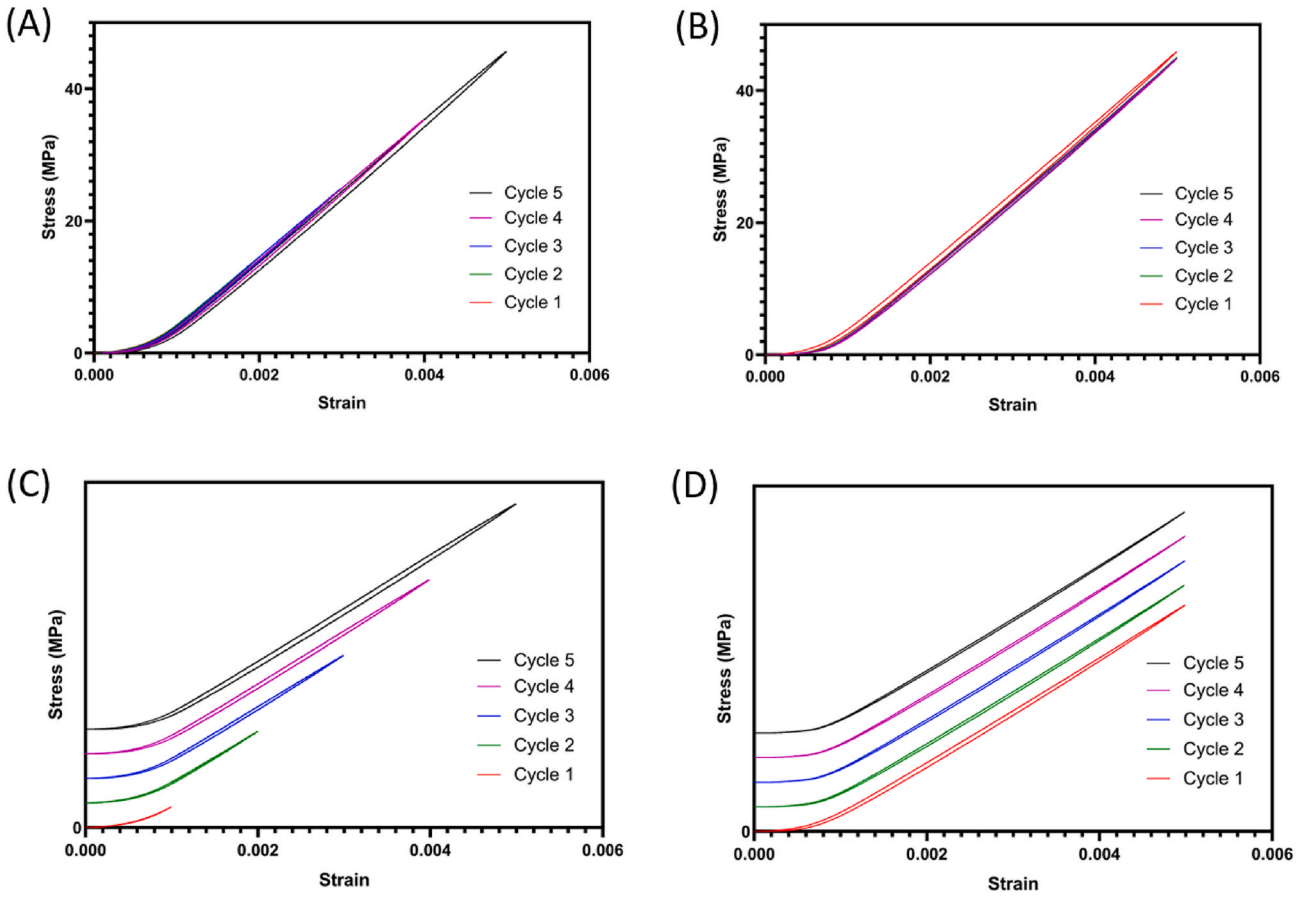

Fig. 10. Dynamic loading test results of porous silicon nitride with 76% porosity: (A) progressive loading; (C) separated cycles from progressive loading; (B) cyclic loading and (D) separated cycles from cyclic loading. Separated cycles are offset vertically for clarity to illustrate evolution of the hysteresis curves. (For interpretation of the references to colour in this figure legend, the reader is referred to the Web version of this article.)

a hysteresis loop was observed. Fig. 10 (B, D) shows the stress vs. strain curve under cyclic loading. Most of the energy dissipation occurred in the first cycle, with little dissipation in the following cycles. Overall, from the dynamic loading test results, we observed there was only a small hysteresis loop, indicating low energy dissipation of porous silicon nitride.

3.5. Mechanical behavior of porous silicon nitride scaffolds under impact

Fig. 11 (D) shows the force vs. time curve during impact from one representative sample. The impact time was less than 1 ms. The average ultimate strength of porous silicon nitride with ~76% porosity was 29.19 ± 4.37 MPa at an impact speed of 1.7 m/s, which is significantly lower than the compressive strength (50.01 ± 1.81 MPa) under quasi-static compression. However, the fracture modes were both 45° plane shear failure, as shown in Fig. 11 (B), which can be theoretically explained by a classic Mohr's circle. In our study, compression may cause a linear fracture, but this will result in failure in a shearing plane, with the 45° plane experiencing the maximum shear stress. In addition, compared to the ultimate strength of bovine trabecular bone [22], the value for porous silicon nitride samples with 76% porosity was higher.

4. Discussion

It is well-known that silicon nitride has excellent mechanical properties and has been therefore widely adopted in novel industrial applications [27]. However, compared to other established biomaterials, it is still a relatively new option for use in medical devices. There is a paucity of reports evaluating its mechanical compatibility to natural bone. In this study, we examined the mechanical properties of both dense and porous silicon nitride. As musculoskeletal loading is dynamic, its impact response and frequency-dependent damping were also evaluated, as these properties are considered important for the long-term function of spinal implants.

Currently, dense silicon nitride is mostly used for spinal implants, such as spinal fusion cages. It is reported that the flexural strength of dense silicon nitride is around 800–1100 MPa with an elastic modulus of around 296–313 GPa [28]. In our study, the elastic modulus was found to be in the same range. Although sufficient strength is required for implant safety, a high elastic modulus may cause stress shielding and lead to bone atrophy [29]. The design of porous structures provides a possible way to reduce the stiffness of implants, but usually at the cost of decreased strength [11]. In this study, we investigated the correlation between mechanical properties and porosity to add valuable data for designing ideal porous implants. The Young's moduli of the dense silicon nitride samples with a density of $\sim 3.26\ \mathrm{g{\cdot}cm^{-3}}$ measured in the present study are significantly higher than Young's modulus of cortical bone and trabecular bone [30–32]. Conversely, the Young's moduli of porous silicon nitride samples with 70% porosity was 14.84 ± 0.91 GPa. This value is only 5% of Young's modulus of dense silicon nitride samples, and it is close to the tissue modulus of an individual trabeculae (14.8 GPa (S.D. 1.4)) measured ultrasonically in the study from Rho et al. [32]. Although the Young's moduli of the porous silicon nitride samples are still higher than the structural modulus of human cancellous bone (from few hundred MPa to 2–3 GPa [33,34]), the porous silicon nitride scaffolds may be beneficial in reduction of stress shielding effect compared to bulk silicon nitride or commonly used metals. Moreover, the porous structures might support the process of new cancellous bone

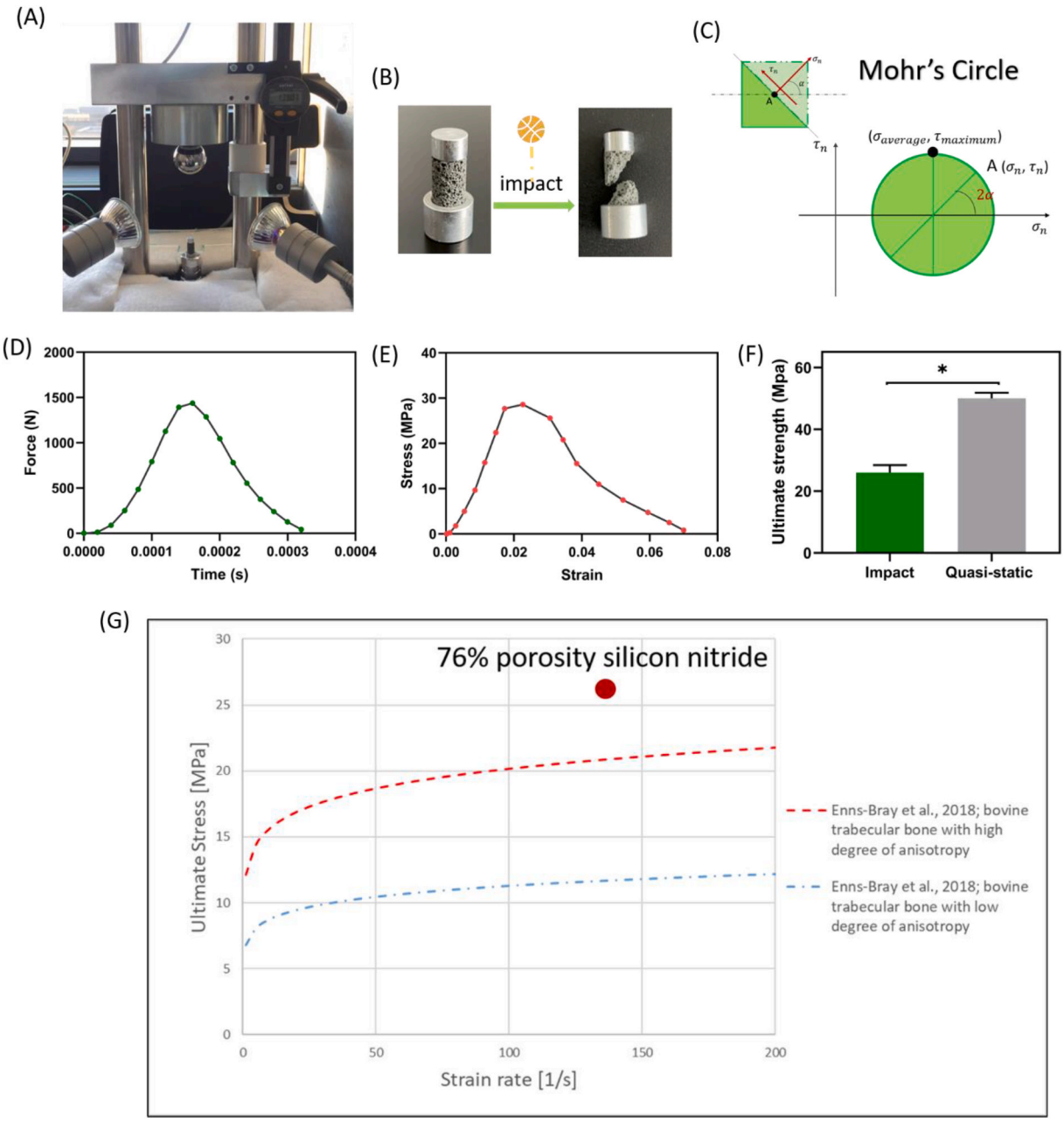

Fig. 11. Drop tower results: (A) drop tower setup; (B) sample before impact and after impact; (C) Mohr's circle representation; (D) Force-time curve of one represent sample; (E) Stress-strain curve of a representative sample, (F) ultimate strength results comparison between drop tower test and quasi-static compression test, and (G) ultimate strength results comparison with bovine trabecular bone tested in the same method by Enns-Bray et al. [22]. Used with permission from Elsevier (copyright 2018).

formation. The compressive strength of the human vertebral bone was reported as 20.99 ± 2.57 kp/cm^2 from the study of Galante et al. [35] in 1970, which corresponds to 2.058 ± 0.252 MPa. Another study more recently also showed a similar axial compressive strength of normal human vertebrae (2.270 ± 1.142 MPa) [36]. Compared to vertebrae, the trabecular bone on femoral neck possessed higher compressive strength, with values from ~5 up to ~35 MPa, depending on bone volume fraction [37]. The compressive strength of porous silicon nitride bioceramic with 70% porosity was 100.35 ± 3.39 MPa. Therefore, as far as we are concerned, it is sufficient for load bearing purpose as a substitute for trabecular bone, especially for trabecular vertebral bone. Since Young's modulus and compressive strength are two key mechanical properties of ceramics, efforts have been made to model the dependence of mechanical properties on the porosity of engineering ceramics [38]. We fitted the experimental data over the range of 65%–80% porosity to the model proposed by Nielsen [21] and obtained the shape factor for silicon nitride. This model has the potential to predict Young's modulus of porous silicon nitride ceramics over a wider porosity range.

Currently, PEEK and titanium alloy are the two main materials employed clinically in fusion cages with worldwide implementation. The ultimate compressive strength of sintered porous titanium with a porosity of 45–75% may reach 24–268 MPa, respectively [39]. Chen et al. [40] compared the mechanical properties between a 3D printed porous titanium cage and a PEEK cage. The results showed that the compressive strength for a titanium cage (70% porosity) was only 65.9 MPa, implying additional structural considerations, whilst for the dense PEEK cage the strength was 94.7 MPa. Another study reported the mechanical properties of porous PEEK and the results showed that the

flexural strength of a porous PEEK with 50% porosity was 21.6 MPa [26]. Compared with these materials, the porous silicon nitride in our study showed a higher compressive strength, which thereby limits risks regarding implant failure.

Ceramics demonstrate unique responses and failure behavior under both impact (shock) and thermal loadings. While the dynamic failure process of ceramics can spread the impact load over a larger area and extend the duration of impact loading, thus reducing the stress on the adjoining structures [41], catastrophic failure is nevertheless to be avoided in implants. Intrinsic material properties, confinement, geometry as well as interfacial conditions are important factors that influence the failure process of a ceramic. Fracture toughness is the main metric to evaluate its ability of a ceramic to resist crack propagation. It is well known that fracture toughness of silicon nitride relies on its grain morphology and can be modulated by controlling the size and amount of large elongated grains (β-Si_3N_4) in a fine-grained matrix. Like whisker-reinforced ceramics, the formation of β-grains in silicon nitride, existing as elongated hexagonal prisms, can toughen the material by crack wake mechanisms including bridging of the crack by unbroken elongated grains and frictional pull-out of elongated grains [42,43]. In our study, the fracture toughness of silicon nitride decreased moderately compared with the change in Young's modulus with porosity. This is related to the microstructure difference between dense and porous silicon nitride. The porous silicon nitride samples exhibited more and larger elongated grains. This is probably because the growth of β-Si_3N_4 is promoted where there is more space available [44]. Notably, the facture toughness of dense silicon nitride was comparable to human cortical bone and the fracture toughness of porous silicon nitride was higher than that of human trabecular bone.

Because rapidly acting forces can cause severe injuries, and slow rate compressive measurements do not predict the behavior of the structures during impact, a drop tower test was introduced to evaluate the impact response of silicon nitride scaffolds [22,45]. This test examined the mechanical behavior of silicon nitride scaffolds at extremely high strain rates, adding valuable data to allow the pre-clinical assessment of potential catastrophic failure modes of the implant or implant-bone interface. The results showed that the average ultimate strength of porous silicon nitride with ~76% porosity was significantly lower under impact conditions than the compressive strength under quasi-static compression. During the drop tower test, the interface between the dropped ball and scaffold created a local stress concentration, which initiated failure of the scaffold. Nevertheless, the ultimate strength of porous silicon nitride was still higher than bovine trabecular bone, previously tested in the same apparatus [22]. Moreover, Kamal et al. [46] investigated the impact behavior of spinal motion segments by a drop tower testing apparatus. The ultimate strength of ovine lumbar spine segments was 19.60 ± 4.8 MPa and the fracture mainly occurred in the body of the vertebra during impact loading. The porous silicon nitride in our study showed a better impact resistance than the ovine vertebrae, which is a favorable consideration for use as spinal spacers and fusion cages.

From the above discussion, porous silicon nitride with decreased elastic modulus may allow for homogeneous stress transfer between an implant and bone. Their strength and fracture toughness are sufficient to maintain the safety of implants and to act as load-bearing substitutes for trabecular bone. The results also showed that altering the porosity of silicon nitride is an efficient way to tailor its mechanical properties, which can be utilized in the pursuit of the design of patient-specific porous implants.

As natural spinal tissues have unique dynamic properties, the damping properties of spinal implants are also relevant. We introduced two testing methods to determine the damping properties of silicon nitride. The first is a direct method that measures energy dissipation, during progressive and cyclic loading. The other method is indirect, measuring variation in the amplitude and frequency of vibration, which are related to the energy dissipated, as in the free damped vibrations test and dynamic mechanical analysis (DMA) test. The results of free damped vibration tests of cantilever beams showed that a silicon nitride beam has a higher damping ratio than a zirconia beam. Ceramics with similar Young's moduli therefore can have different energy dissipating capacities. However, both dense silicon nitride and zirconia possessed low damping ratios, which are both much lower than the natural vertebral bone or intervertebral discs [47,48]. Another study using the free decay vibration test reported the damping of selective-laser-melted NiTi for medical implants [49]. Their results showed that the two NiTi cantilevers showed a damping ratio of ~0.03 at temperatures below austenite start, maximal values of up to 0.04 in the transformation regions and low values of ~0.005 above austenite. These values were higher than the damping ratio of the silicon nitride beam in our study. However, since the sample size of the NiTi was about 8 times bigger than the silicon nitride beam in our study, it is difficult to compare the results directly. Nevertheless, it is well-known that most dense ceramics and metals have low damping properties [50]. As many studies have demonstrated a positive correlation between damping and porosity [51–53], increasing porosity of silicon nitride may improve its damping characteristics. However, our results for the porous silicon nitride from either the DMA or dynamic loading tests showed a low energy dissipation ability. Although the porosity was up to 70%, there was a high ratio of closed pores formed by the elongated grains. This may have negatively influenced the energy dissipation capacity of the porous silicon nitride samples.

More efforts are needed to improve the damping properties of silicon nitride. In general, energy dissipation is attributed to intrinsic material damping, elastic buckling, or plastic deformation, and both the material and structure appear to affect the energy dissipation [54]. One of the most common methods to improve the damping properties of a system is to add extra tuned mass dampers, consisting of mass, spring, and damping elements. However, it is impractical to add dampers to an implant. Therefore, a better method is to optimize the structural properties to control damping. Cellular structures including stochastic foams and periodic cells are widely employed as energy absorption structures [55]. Schroer et al. [54] investigated the deformation behavior and energy absorption capability of ceramic-polymer composite micro-lattices under cyclic loading and the results showed that honeycomb structures dissipate the highest amount of specific energy compared to hexagonal, cubic, and tetrahedral structures. Therefore, optimization of the structure is an effective method to tailor the damping capacity. This could be considered in the design of silicon nitride-based spinal implants. Other possible ways to increase the damping properties of silicon nitride-based implants may include adding an energy dissipating additive into the silicon nitride, fabricating composite materials or using disspiative layers and coatings.

5. Conclusion

This study evaluated the correlation between mechanical properties and porosity in silicon nitride bioceramics and the results showed that Young's modulus and compressive strength decreased non-linearly as porosity increased. Additionally, the Young's modulus of a porous silicon nitride beam with 70% porosity (26.26 ± 1.23 GPa) was 11 times lower than that of a dense silicon nitride beam (298.45 ± 1.08 GPa) measured ultrasonically, whilst the fracture toughness only decreased 5 times. Both the fracture toughness (1.06 ± 0.06 MPa·$m^{1/2}$) and the compressive strength (100.35 ± 3.39 MPa) of the porous silicon nitride samples (~70% porosity) are sufficient to act as load-bearing substitutes for trabecular bone and to maintain the safety of implants. As quasi-static compressive tests do not predict the behavior of structures during impact, a drop tower test was employed to evaluate the impact response of porous silicon nitride scaffolds. The results showed that the average ultimate strength of the scaffolds at an impact at a speed of 1.7 m/s was significantly lower than the compressive strength under quasi-

static compression. Nevertheless, this value is still competitive to that of trabecular bone. Therefore, the above results show that altering the porosity of silicon nitride is an efficient way to tailor its mechanical properties, towards providing a Young's modulus similar to that of natural bone while maintaining adequate strength and toughness. Furthermore, the dynamic properties of dense silicon nitride and porous silicon nitride were evaluated and both showed low damping properties. Their energy dissipated ability was still significantly lower than natural spinal tissues. Further design and development may improve this damping capacity, leading to silicon nitride implants that are bone compatible yet strong and which contribute to the adequate dissipation of energy during impact or vibration loading.

Declaration of competing interest

The authors declare that they have no known competing financial interests or personal relationships that could have appeared to influence the work reported in this paper.

Acknowledgement

This project has received funding from the European Union's Horizon 2020 research and innovation program under the Marie Skłodowska-Curie grant agreement No.812765. The authors acknowledge support of the Scientific Center for Optical and Electron Microscopy ScopeM of the Swiss Federal Institute of Technology ETHZ. The authors thank Roland Bächtold from EMPA for his support with the sonic excitation test and single-edge V-notch beam test and Peter Schwilch from ETH Zurich for his help regarding drop tower test. The authors also acknowledge Dr. Bryan McEntire (SINTX Technologies, USA) for his kind assistance with providing samples.

References

[1] A.Y. Jim, L. Sue, Myhre, B.S. Bal, Radiographic follow-up of transforaminal lumbar fusion with silicon nitride spacers A case report of two patients, Journal of Musculoskeletal Disorders and Treatment 2 (1) (2016) 8.
[2] R.F.M.R. Kersten, G. Wu, B. Pouran, A.J. van der Veen, H.H. Weinans, A. de Gast, F. C. Oner, S.M. van Gaalen, Comparison of polyetheretherketone versus silicon nitride intervertebral spinal spacers in a caprine model, J. Biomed. Mater. Res. B 107 (3) (2019) 688–699.
[3] B.S. Bal, M.N. Rahaman, Orthopedic applications of silicon nitride ceramics, Acta Biomater. 8 (8) (2012) 2889–2898.
[4] C. Sorrell, P. Hardcastle, R. Druitt, C. Howlett, E. McCartney, Results of 15-Year Clinical Study of Reaction Bonded Silicon Nitride Intervertebral Spacers, 7th World Biomaterials Congress, 2004, p. 1872.
[5] R.J. Mobbs, P.J. Rao, K. Phan, P. Hardcastle, W.J. Choy, E.R. McCartney, R. K. Druitt, C.A.L. Mouatt, C.C. Sorrell, Anterior lumbar interbody fusion using reaction bonded silicon nitride implants: long-term case series of the first synthetic anterior lumbar interbody fusion spacer implanted in humans, World Neurosurg 120 (2018) 256–264.
[6] R.F.M.R. Kersten, S.M. van Gaalen, M.P. Arts, K.C.B. Roes, A. de Gast, T.P. Corbin, F.C. Oner, The SNAP trial: a double blind multi-center randomized controlled trial of a silicon nitride versus a PEEK cage in transforaminal lumbar interbody fusion in patients with symptomatic degenerative lumbar disc disorders: study protocol, Bmc Musculoskel Dis 15 (2014).
[7] B.J. McEntire, G. Maslin, B.S. Bal, Two-year results of a double-blind multicenter randomized controlled non-inferiority trial of polyetheretherketone (PEEK) versus silicon nitride spinal fusion cages in patients with symptomatic degenerative lumbar disc disorders, J Spine Surg 6 (3) (2020) 523–540.
[8] M.P. Arts, J.F.C. Wolfs, T.P. Corbin, Porous silicon nitride spacers versus PEEK cages for anterior cervical discectomy and fusion: clinical and radiological results of a single-blinded randomized controlled trial, Eur. Spine J. 26 (9) (2017) 2372–2379.
[9] E. Babaie, S.B. Bhaduri, Fabrication aspects of porous biomaterials in orthopedic applications: a review, ACS Biomater. Sci. Eng. 4 (1) (2018) 1–39.
[10] S.L. Wu, X.M. Liu, K.W.K. Yeung, C.S. Liu, X.J. Yang, Biomimetic porous scaffolds for bone tissue engineering, Mat Sci Eng R 80 (2014) 1–36.
[11] C.N. Sun, L. Wang, J.F. Kang, D.C. Li, Z.M. Jin, Biomechanical optimization of elastic modulus distribution in porous femoral stem for artificial hip joints, J Bionic Eng 15 (4) (2018) 693–702.
[12] L. Yuan, S.L. Ding, C.E. Wen, Additive manufacturing technology for porous metal implant applications and triple minimal surface structures: a review, Bioact Mater 4 (2019) 56–70.
[13] P. Boughton, D. Ferris, A.J. Ruys, A ceramic-polymer functionally graded material: a novel disk prosthesis, 25th Annual Conference on Composites, Advanced Ceramics, Materials, and Structures: B 22 (4) (2001) 593–600.
[14] G. Marini, G. Huber, K. Puschel, S.J. Ferguson, Nonlinear dynamics of the human lumbar intervertebral disc, J. Biomech. 48 (3) (2015) 479–488.
[15] G. Marini, S.J. Ferguson, Nonlinear numerical analysis of the structural response of the intervertebral disc to impact loading, Comput Method Biomec 17 (9) (2014) 1002–1011.
[16] G. Marini, G. Huber, K. Puschel, S.J. Ferguson, A 1-D model of the nonlinear dynamics of the human lumbar intervertebral disc, J. Sound Vib. 387 (2017) 194–206.
[17] S.A. Gonzalez-Blohm, J.J. Doulgeris, W.E. Lee, T.M. Shea, K. Aghayev, F.D. Vrionis, The current testing protocols for biomechanical evaluation of lumbar spinal implants in laboratory setting: a review of the literature, 2015, BioMed Res. Int. 2015 (2015) 15, 506181.
[18] Z. Kiral, B.M. Icten, B.G. Kiral, Effect of impact failure on the damping characteristics of beam-like composite structures, Compos. B Eng. 43 (8) (2012) 3053–3060.
[19] I.R. Henriques, L.A. Borges, M.F. Costa, B.G. Soares, D.A. Castello, Comparisons of complex modulus provided by different DMA, Polym. Test. 72 (2018) 394–406.
[20] G. Blugan, M. Hadad, J. Janczak-Rusch, J. Kuebler, T. Graule, Fractography, mechanical properties, and microstructure of commercial silicon nitride-titanium nitride composites, J. Am. Ceram. Soc. 88 (4) (2005) 926–933.
[21] L.F. Nielsen, Elasticity and damping of porous materials and impregnated materials, J. Am. Ceram. Soc. 67 (2) (1984) 93–98.
[22] W.S. Enns-Bray, S.J. Ferguson, B. Helgason, Strain rate dependency of bovine trabecular bone under impact loading at sideways fall velocity, J. Biomech. 75 (2018) 46–52.
[23] B. Katona, A. Szlancsik, T. Tabi, I.N. Orbulov, Compressive characteristics and low frequency damping of aluminium matrix syntactic foams, Mat Sci Eng a-Struct 739 (2019) 140–148.
[24] L.F.C.P. Lima, A.L.E. Godoy, E.N.S. Muccillo, Elastic modulus of porous Ce-TZP ceramics, Mater. Lett. 58 (1–2) (2004) 172–175.
[25] X.X. Zhang, H.W. Hou, L.S. Wei, Z.X. Chen, W.T. Wei, L. Geng, High damping capacity in porous NiTi alloy with bimodal pore architecture, J. Alloys Compd. 550 (2013) 297–301.
[26] B.C. Landy, S.B. VanGordon, P.S. McFetridge, V.I. Sikavitsas, M. Jarman-Smith, Mechanical and in vitro investigation of a porous PEEK foam for medical device implants, J Appl Biomater Func 11 (1) (2013) 35–44.
[27] M.H. Bocanegra-Bernal, B. Matovic, Mechanical properties of silicon nitride-based ceramics and its use in structural applications at high temperatures, Mat Sci Eng a-Struct 527 (6) (2010) 1314–1338.
[28] B.J. McEntire, B.S. Bal, M.N. Rahaman, J. Chevalier, G. Pezzotti, Ceramics and ceramic coatings in orthopaedics, J. Eur. Ceram. Soc. 35 (16) (2015) 4327–4369.
[29] M. Niinomi, M. Nakai, Titanium-based biomaterials for preventing stress shielding between implant devices and bone, Int J Biomater 2011 (2011).
[30] D. Wu, P. Isaksson, S.J. Ferguson, C. Persson, Young's modulus of trabecular bone at the tissue level: a review, Acta Biomater. 78 (2018) 1–12.
[31] M. Cuppone, B.B. Seedhom, E. Berry, A.E. Ostell, The longitudinal Young's modulus of cortical bone in the midshaft of human femur and its correlation with CT scanning data, Calcif. Tissue Int. 74 (3) (2004) 302–309.
[32] J.Y. Rho, R.B. Ashman, C.H. Turner, Youngs modulus of trabecular and cortical bone material - ultrasonic and microtensile measurements, J. Biomech. 26 (2) (1993) 111–119.
[33] R.B. Ashman, J.Y. Rho, Elastic-modulus of trabecular bone material, J. Biomech. 21 (3) (1988) 177–181.
[34] X. Banse, T.J. Sims, A.J. Bailey, Mechanical properties of adult vertebral cancellous bone: correlation with collagen intermolecular cross-links, J. Bone Miner. Res. 17 (9) (2002) 1621–1628.
[35] J. Galante, W. Rostoker, R.D. Ray, Physical properties of trabecular bone, Calcif. Tissue Res. 5 (3) (1970) 236–&.
[36] R. Cesar, T.P. Leivas, C.A.M. Pereira, R.S. Boffa, R. Guarniero, R.B.d.M. Reiff, A. Mandeli Netto, C.A. Fortulan, J.M.D.d.A. Rollo, Axial compressive strength of human vertebrae trabecular bones classified as normal, osteopenic and osteoporotic by quantitative ultrasonometry of calcaneus, Research on Biomedical Engineering 33 (2) (2017) 91–96.
[37] A. Sanyal, A. Gupta, H.H. Bayraktar, R.Y. Kwon, T.M. Keaveny, Shear strength behavior of human trabecular bone, J. Biomech. 45 (15) (2012) 2513–2519.
[38] L. Zhang, K.W. Gao, A. Elias, Z.G. Dong, W.X. Chen, Porosity dependence of elastic modulus of porous Cr3C2 ceramics, Ceram. Int. 40 (1) (2014) 191–198.
[39] B. Dabrowski, W. Swieszkowski, D. Godlinski, K.J. Kurzydlowski, Highly porous titanium scaffolds for orthopaedic applications, J. Biomed. Mater. Res. B 95b (1) (2010) 53–61.
[40] C. Chen, Y. Hao, X. Bai, J.J. Ni, S.M. Chung, F. Liu, I.S. Lee, 3D printed porous Ti6Al4V cage: effects of additive angle on surface properties and biocompatibility; bone ingrowth in Beagle tibia model, Mater. Des. 175 (2019).
[41] W.W. Chen, A.M. Rajendran, B. Song, X. Nie, Dynamic fracture of ceramics in armor applications, J. Am. Ceram. Soc. 90 (4) (2007) 1005–1018.
[42] X.H. Tian, J. Zhao, Z.B. Wang, X.H. Liu, Design and fabrication of Si3N4/(W, Ti)C graded nano-composite ceramic tool materials, Ceram. Int. 42 (12) (2016) 13497–13506.
[43] N. Kondo, Y. Suzuki, T. Ohji, Superplastic sinter-forging of silicon nitride with anisotropic microstructure formation, J. Am. Ceram. Soc. 82 (4) (1999) 1067–1069.

[44] J.F. Yang, T. Ohji, S. Kanzaki, A. Diaz, S. Hampshire, Microstructure and mechanical properties of silicon nitride ceramics with controlled porosity, J. Am. Ceram. Soc. 85 (6) (2002) 1512–1516.
[45] L.V. Burgin, R.M. Aspden, A drop tower for controlled impact testing of biological tissues, Med. Eng. Phys. 29 (4) (2007) 525–530.
[46] S. Kamal, A. Hashemi, Design and fabrication of a drop tower testing apparatus to investigate the impact behavior of spinal motion segments, Arch Bone Jt Surg-Ab 8 (6) (2020) 682–688.
[47] G.D. Qiao, S. Rahmatalla, Identification of damping and stiffness parameters of cervical and lumbar spines of supine humans under vertical whole-body vibration, J Low Freq Noise V A 39 (1) (2020) 59–71.
[48] L.X. Guo, E.C. Teo, K.K. Lee, Q.H. Zhang, Vibration characteristics of the human spine under axial cyclic loads: effect of frequency and damping, Spine 30 (6) (2005) 631–637.
[49] M. de Wild, F. Meier, T. Bormann, C.B.C. Howald, B. Muller, Damping of selective-laser-melted NiTi for medical implants, J. Mater. Eng. Perform. 23 (7) (2014) 2614–2619.
[50] J. Zhang, R.J. Perez, E.J. Lavernia, Documentation of damping capacity of metallic, ceramic and metal-matrix composite-materials, J. Mater. Sci. 28 (9) (1993) 2395–2404.
[51] J. Zhang, M.N. Gungor, E.J. Lavernia, The effect of porosity on the microstructural damping response of 6061 aluminum-alloy, J. Mater. Sci. 28 (6) (1993) 1515–1524.
[52] J.C. Yin, J.H. Zhang, Y. Zhang, W.Q. Wang, Porosity, mechanical properties, and damping ratio of particulate-filled polymer composite for precision machine tools, J. Appl. Polym. Sci. 134 (6) (2017).
[53] X. Zhou, F. Cao, J.H. Li, W. Shen, J.L. Liu, Synthesis of porous Co3O4/C/(Mg, Ca)O nanocomposites by natural biological template for application in dynamic damping absorption, J. Alloys Compd. 688 (2016) 354–361.
[54] A. Schroer, J.M. Wheeler, R. Schwaiger, Deformation behavior and energy absorption capability of polymer and ceramic-polymer composite microlattices under cyclic loading, J. Mater. Res. 33 (3) (2018) 274–289.
[55] Y.L. Liu, T.A. Schaedler, A.J. Jacobsen, X. Chen, Quasi-static energy absorption of hollow microlattice structures, Compos. B Eng. 67 (2014) 39–49.
[56] R.K. Roeder, G.L. Converse, R.J. Kane, W.M. Yue, Hydroxyapatite-reinforced polymer biocomposites for synthetic bone substitutes, Jom-Us 60 (3) (2008) 38–45.